



Universiteit
Leiden
The Netherlands

Self-assembly of flexible and rigid structures: from colloidal molecules to lattices

Shelke, Y.P.

Citation

Shelke, Y. P. (2023, October 24). *Self-assembly of flexible and rigid structures: from colloidal molecules to lattices. Casimir PhD Series*. Retrieved from <https://hdl.handle.net/1887/3645933>

Version: Publisher's Version

License: [Licence agreement concerning inclusion of doctoral thesis in the Institutional Repository of the University of Leiden](#)

Downloaded from: <https://hdl.handle.net/1887/3645933>

Note: To cite this publication please use the final published version (if applicable).

Chapter 4

Self Assembly of Flexible Colloidal Lattices

Abstract

DNA-grafted colloids have emerged as a promising model for understanding the crystallization process of atoms or molecules. However, the formation of rigid colloidal bonds during nucleation and growth processes of DNA grafted colloids typically leads to the development of rigid colloidal lattices. In this work, we self-assemble flexible colloidal square lattices using a binary mixture of colloids functionalized with complementary surface-mobile DNA linkers. We follow their assembly pathways and observe the development of flexible colloidal lattices *in-situ* from spheres with complementary DNA linkers and size ratio $\alpha_{s-s} = 1$ and 1.65, as well as spheres and cubes with size ratio $\alpha_{s-c} = 1.23$ to gain insights into their nucleation and growth. We find that flexibility of the DNA bonds permits the structures to reconfigure during lattice growth and optimize the number of bonds and their location, which results in flexible colloidal square lattices. We enhance the accuracy and yield of the desired lattice by steering the pathway towards a specific coordination number by leveraging an anisotropic particle shape as well as the particle number ratio and size ratio. The directional bonding and constrained flexibility of the sphere-cube system results in the most ordered 2D crystalline lattices. These lattices may be helpful in making flexible electronic materials and photonic crystals with tunable photonic properties.

4.1 Introduction

Bond flexibility significantly influences the mechanical, thermal and electronic properties of the materials.[1–6] It enables rearrangements between the bound elements, crucial for optimizing the number of bonds between the constituent elements and correcting errors, and thus, ultimately, reaching the thermodynamically favorable states.[7] Moreover, after assembly, the ability to rearrange is key to heat and sound transport in materials, and in the presence of global floppy modes enables conformational changes which are a prerequisite for creating functional colloidal materials and devices in the future.

Although theoretical and numerical studies often assume rearrangements being possible after bonding, in experiments this is often not the case. In atomic and molecular systems other factors such as bond directionality and valence dominate, and most colloidal bonds do not allow rearrangements due to surface inhomogeneities which trap their configuration in metastable states. This restricts an experimental comparison with theoretical predictions, singling out the effect of bond flexibility, and reaching the thermodynamically most favorable state.

Rearranging bonds have recently been experimentally realized in colloidal systems.[8–11] Colloidal particles functionalized by DNA linkers covalently bound to their surface have been shown to allow rearrangements in a narrow temperature range just below the melting temperature of the DNA, which creates transient, weak bonds. These particles were then shown to crystallize into different lattice structures that are otherwise not achievable by DNA-based interactions.[12, 13] An alternative approach that provides bond flexibility over a wide temperature range uses DNA linkers that are mobile on the colloid surface.[9, 11] This can be realized either by placing the linkers on fluid droplets or inside lipid bilayers supported by solid colloidal particles. In addition, the bond strength for surface mobile DNA linkers can be set to obtain irreversible bonds, whose strength can further be tuned by temperature *in situ*, while surface bound DNA linkers require reversible and hence weak bonds to achieve flexibility. This strategy has been employed to create a variety of flexible structures ranging from flexible chains to rings and colloidal molecules with and without limited angular range up to foldable structures.[7, 10, 14–17] However, the self-assembly of larger periodic and flexible structures such as floppy crystalline lattices has not been achieved with colloids with surface-mobile linkers yet, and the impact of rearranging bonds on the kinetics of lattice formation and the final crystal structures are unknown.

Here, we experimentally study the nucleation and growth of floppy crystalline structures from a binary mixture of colloidal particle with flexible bonds. We investigate the influence of bond flexibility on nucleation and growth for equal sized spherical particles, and find that their ability to rearrange enhances the formation of two-dimensional square lattices. Utilizing *in situ* observations with confocal and bright field microscopy, we map out their evolution to gain a deeper understanding of the pathways leading to the formation of these flexible colloidal lattices. We leverage particle size ratio and shape to guide the self-assembly towards square lattices with high fidelity. Our findings may serve as a tool to design innovative flexible materials with tailored properties that may be employed as sensors, actuators and in smart devices and machines.

4.2 Materials and Methods

4.2.1 Experimental Section

Materials

Silica microspheres of diameters $1.25 \pm 0.05 \mu\text{m}$, $1.55 \pm 0.05 \mu\text{m}$, $2.06 \pm 0.05 \mu\text{m}$, in 5 wt/v% suspension were purchased from Microparticles GmbH. Silica particles of diameter $0.66 \pm 0.01 \mu\text{m}$ were synthesized by a Stöber method. Sodium chloride, Ethanol, Sodium hydroxide, Ammonium hydroxide (28-30 v/v%), Iron(III) Chloride Hexahydrate ($\text{FeCl}_3 \cdot 6\text{H}_2\text{O}$), Tetraethyl orthosilicate (TEOS), 4-(2-hydroxyethyl)-1-piperazineethanesulfonic acid (HEPES), trimethoxysilyl propyl methacrylate (TPM), were purchased from Sigma-Aldrich and used as received. 1,2-dioleoyl-*sn*-glycero-3-phosphocholine (DOPC), 1,2-dioleoyl-*sn*-glycero-3-phosphoethanolamine-N-[methoxy(polyethylene glycol)-2000] (DOPE-PEG2000), 1,2-dioleoyl-*sn*-glycero-3-phosphoethanolamine-N-(lis-samine rhodamine B sulfonyl) (DOPE-Rhodamine) and dye 23-(dipyrrom-etheneboron difluoride)-24-nor-cholesterol (TopFluor-Cholesterol) were obtained from Avanti Polar Lipids, Inc.. We used Milli-Q water for all experiments. DNA strands were purchased from Eurogentec. The sequences of DNA used were:

Strand A: Double Stearyl-HEG-5'-TT-TAT-CGC-TAC-CCT-TCG-CAC-AGT-CAC-CTT-CGC-ACA-GTC-ACA-TTC-AGA-GAG-CCC-TGT-CTA-GAG-AGC-CCT-GCC-TTA-CGA-*G-T-A-G-A-A-3'-6FAM*,

Strand B: Double Stearyl-HEG-5'-TT-TAT-CGC-TAC-CCT-TCG-CAC-AGT-CAC-CTT-CGC-ACA-GTC-ACA-TTC-AGA-GAG-CCC-TGT-CTA-GAG-AGC-CCT-GCC-TTA-CGA-*T-T-C-T-A-C-3'-Cy3*,

Strand C: 5'-TCG-TAA-GGC-AGG-GCT-CTC-TAG-ACA-GGG-CTC-TCT-GAA-TGT-GAC-TGT-GCG-AAG-GTG-ACT-GTG-CGA-AGG-GTA-GCG-ATT-TT-3',

Strand D: Double Stearyl-5TT-TAT-CGC-TAC-CCT-TCG-CAC-AGT-CAA-TCT-AGA-GAG-CCC-TGC-CTT-ACG-A and Strand E: TCG-TAA-GGC-AGG-GCT-CTC-TAG-ATT-GAC-TGT-GCG-AAG-GGT-AGC-GAT-TTT. The linker sequence in strand A and strand B is italicised.

Synthesis of Silica Cubes

The hematite cubes of edge length $1.08 \pm 0.04 \mu\text{m}$ were synthesized following reference[18] and coated with a $0.135 \mu\text{m}$ silica layer using the process described in reference[19]. It resulted in hematite-silica core-shell cubes of edge length $1.35 \pm 0.07 \mu\text{m}$. In a typical synthesis of hematite cubes, 100 ml of aqueous 2M $\text{FeCl}_3 \cdot 6\text{H}_2\text{O}$ was prepared in a 500 ml Pyrex bottle. Next, 100 ml of 5M NaOH solution were added while stirring at 1000 rpm for 51 seconds. Then, the mixture was stirred continuously for another 10 minutes and subsequently placed in a pre-heated oven and left undisturbed at 100°C for 8 days. The resulting hematite cubes were washed several times using centrifugation and redispersion in milliQ water. To coat them with a thick $0.135 \mu\text{m}$ layer of silica, 100 ml of ethanol and 0.6 g of synthesized cubes were mixed under sonication and mechanical stirring

in a 2-neck round bottom flask at 50 °C. Subsequently, 5 ml of water, 15 ml of ammonium hydroxide solution and TEOS were poured into the reaction flask and allowed to coat the particles for 5hr under the same conditions. Next, the silica layer was allowed to grow on the cube's surface for 5h. The resulting particles were first washed three times with ethanol and then three times with water to remove unreacted chemicals by repeated centrifugation and redispersion.

Preparation of Small Unilamellar Vesicles (SUVs)

Small unilamellar vesicles (SUVs) were prepared using a protocol described in reference[20]. For the preparation of SUVs, we used 77 μl of 25 g/L DOPC, 7.34 μl of 10 g/L DOPE PEG 2000, and 2 μl of either 1 g/L dye DOPE-rhodamine or 2 μl of 1 g/L TopFluor-Cholesterol dissolved in chloroform were mixed together in a glass vial. Subsequently, the lipid mixture was dried for at least 2 hrs in a desiccator (Kartell) attached to a vacuum pump (KNF LABOPORT N816.3KT.18). Then, 1 ml of buffer solution consisting of 50 mM NaCl and 10 mM HEPES at pH 7.4 was added to the dried lipid. The prepared solution was vortexed for 30 min during which the solution became turbid indicating the formation of giant multilamellar vesicles. The dispersion of giant multilamellar vesicles was extruded with a Avanti Polar Lipids mini extruder 21 times through a 50 nm polycarbonate membrane supported with filter paper to achieve SUV formation. The prepared SUVs were stored in the fridge at 4 °C and used for up to 3 days.

DNA Hybridization

We used double stranded DNA with a complementary 6 base-paires single stranded end to which we refer to as "linker" and inert double-stranded DNA strands for bonding and stabilizing the colloids, respectively. Prior to use, single strand DNA was hybridized with the complementary backbone to make linker DNA. Strand A was hybridized with strand C to yield double-stranded linker DNA, strand B with strand C to obtain the complementary double-stranded linker DNA, and strand D with strand E to create double-stranded inert DNA (DNA strands are listed in the materials section). For hybridization, we typically mixed 10 μl of 20 μM single strands and 10 μl of 20 μM complementary backbone in 90 μl buffer (200mM NaCl, 10mM HEPES, at pH 7.4) solution. The DNA solutions were placed in a preheated oven at 94 °C for 30 minutes. The oven then was switched off and allowed to cool slowly overnight. After cooling, the hybridized DNA strands were stored at 4 °C and used for up to 2 months.

Functionalization of Colloidal Particles with a Lipid Bilayer Containing Linker and Inert DNA

To coat particles with a lipid bilayer we used a 25:1 surface ratio of SUVs to particles. We maintained the same surface area ratio of SUVs to particles when coating differently sized particles. Typically, for 1 μm particles, we use 100 μl of 0.25 wt/v% particles in Milli-Q water and mixed them with 48 μm 0.5 g/L SUVs. Then, the dispersion was rotated at 8 rpm for 1h. During this period, SUVs

collide, burst, spread and form a bilayer on the particles' surface. Then, the coated particles were centrifuged at 800 rpm for 2-5 min and the supernatant containing excess SUVs was removed using a micropipette. Subsequently, linker DNA was added to the particles at a concentration of 2×10^4 labeled with dye cyanine 3 (Cy3) (magenta) and 4×10^4 labeled with dye ATTO488 (green), respectively. We employed three combinations of particles: 1) equal sized spheres of $2.06 \pm 0.05 \mu\text{m}$ diameter, 2) unequal sized spheres of $2.06 \pm 0.05 \mu\text{m}$ and $1.25 \pm 0.05 \mu\text{m}$ diameter, and 3) $1.66 \pm 0.05 \mu\text{m}$ spheres and $1.35 \pm 0.07 \mu\text{m}$ cubes. Inert DNA at a nominal concentration of 5×10^4 DNA strands/ μm^2 was added to all particles suspensions. The suspensions were then rotated for another 1h. Thereafter, each suspension was centrifuged and washed 2 times with a 50 mM NaCl HEPES buffer.

Sample Preparation and Imaging

For all self-assembly experiments, $2.06 \pm 0.05 \mu\text{m}$ spheres and $2.06 \pm 0.05 \mu\text{m}$ spheres a number ratio of 1:1, $2.06 \pm 0.05 \mu\text{m}$ spheres and $1.25 \pm 0.05 \mu\text{m}$ spheres a number ratio of 1.2:1, $1.66 \pm 0.05 \mu\text{m}$ spheres and $1.35 \pm 0.07 \mu\text{m}$ cubes a number ratio of 1:1 was maintained. Polyacrylamide (PAA) coated coverslips were used as substrates and coated with PAA by following the protocol in reference[14]. In a 1.5 ml vial, μl of functionalized $1 \mu\text{m}$ spherical particles and $2.5 \mu\text{l}$ of cubic particles were combined with 500 μl buffer solution of 50 mM NaCl and 10 mM HEPES at pH 7.4. The mixture was then transferred to a customized sample holder and allowed to self-assemble and while being captured with brightfield or confocal microscopy over time upto 2 hrs. During self-assembly sample temperature was maintained $23.0 \pm 0.7^\circ\text{C}$. Images and videos were captured with a Nikon inverted TI-E microscope equipped with an A1 confocal scan head and Prime BSI Express camera (Teledyne Photometrics) for capturing the sample evolution in brightfield mode. The images were taken with a 60x oil objective (N.A. 1.4) at frame rates of up to 25 fps.

Particles Detection and Image Analysis

To extract x and y coordinates from TIF images, the Hough Circles detection technique was used. After detecting the particles, if particles were found to be within a predetermined distance from each other, they were considered to be connected and grouped according to their size. We refer to these connected particles as 'clusters'. To further examine clusters of specific sizes, and demonstrate the connectivity and relationships among particles in each cluster, we generated adjacency matrices for each specific cluster size. This process generates the unique adjacency matrices for differently shaped clusters of the same size. Further, by computing the unique eigenvalues of corresponding adjacency matrices of each cluster type of same size, we subcategorized the clusters into distinct types based on their eigenvalues.

4.3 Results and Discussion

4.3.1 Self-assembly of Flexible Colloidal Lattices

To study the influence of rearranging bonds between colloidal particles on nucleation and growth, as well as the final structure, we explore binary colloidal systems equipped with complementary surface mobile DNA linkers. To do so, we used a method developed by some of us with some modifications.[9, 10, 20] To achieve flexible bonds, the particles were first coated with a lipid bilayer. Subsequently we functionalized them by embedding complementary and inert DNA sequences that consist of cholesterol-anchored dsDNA strands with and without a 6 bp single stranded end, respectively, in the lipid bilayer on their surfaces. We selected conditions where the lipid bilayer is in the fluid phase, thereby allowing the DNA to diffuse across the lipid bilayer and form rearranging bonds between colloids. We chose to study and compare three combinations of complementarily functionalized colloidal particle systems: 1) spheres of equal size with a diameter of $2.06 \pm 0.05 \mu\text{m}$ and $2.06 \pm 0.05 \mu\text{m}$ sphere to sphere size ratio $\alpha_{s-s} = 1$, 2) unequal sized spheres with $2.06 \pm 0.05 \mu\text{m}$ and $1.25 \pm 0.05 \mu\text{m}$ diameter and thus with $\alpha_{s-s} = 1.65$, and 3) spheres with diameter $1.66 \pm 0.05 \mu\text{m}$ and cubes with an edge length of $1.35 \pm 0.07 \mu\text{m}$ and thus with a spheres to cubes edge length ratio $\alpha_{s-c} = 1.23$.

The growth of colloidal lattices in binary DNA-coated colloidal systems is a complex process influenced by the particles' size, shape, and number ratio. Understanding these factors and the effect of bond flexibility on the growth of lattices offers valuable insights into the design and control of colloidal materials. We therefore started by selecting a simple experimental system of binary mixtures of mobile DNA-coated colloids of equal sized spheres ($\alpha_{s-s} = 1$) at equal number ratio (see methods section). We observed that linker DNA concentration, linker DNA length and temperature, significantly influences the binding process, flexibility and melting temperature. We used 6 bp linker length DNA for all experiments which have a melting temperature $\approx 25^\circ\text{C}$ due to low binding strength and therefore, we carefully maintained the sample temperature at $23.0 \pm 0.7^\circ\text{C}$ using a temperature controlled water bath (Julabo) equipped with a Pt100 sensor that was inserted into the sample cell. To identify the optimal concentration of linkers DNA for flexible yet effective binding of particles, we carried out experiments using various concentrations of linker DNA on $2.06 \pm 0.05 \mu\text{m}$ particles, while keeping the linker DNA concentration on the complementarily functionalized particles of the same size fixed at 5×10^4 DNA strands/ μm^2 , as shown in Table 4.1. Additionally, we kept the inert DNA concentration constant for both particles. We discovered that DNA concentrations of 2×10^4 DNA strands/ μm^2 and 5×10^4 DNA strands/ μm^2 on the two complementarily functionalized particles with diameter $2.06 \pm 0.05 \mu\text{m}$ was optimal for achieving both good binding and flexibility of bonds.

We investigate the effect of flexible bonds on the growth of two-dimensional (2D) flexible colloidal lattices from a binary mixture of surface mobile DNA-coated colloids with for equal-sized spheres with size ratio $\alpha_{s-s} = 1$. We monitored their self-assembly over a period of 3600 seconds as seen in the microscope snapshot in Figure 4.1. Intriguingly, well-ordered structures with particles arranged in an AB square lattice emerged. The majority of the single particles was incorporated into

Results and Discussion

Table 4.1: Effect of linker DNA concentration on binding probability and flexibility for equal sized spheres of $2.06 \pm 0.05 \mu\text{m}$ diameter (size ratio $\alpha_{s-s} = 1$) at equal number ratio. The DNA concentration was varied on one of the particles species and kept fixed at 5×10^4 DNA strands/ μm^2 on the another.

ssDNA length (bp)	DNA concentration (strands/ μm^2)	number of bonds per particles	bond type
6	1×10^3	none	none
	2×10^3	none	none
	5×10^3	none	none
	1×10^4	1-2	flexible
	2×10^4	1-5	flexible
	5×10^4	1-5	limited flexibility
	1×10^5	1-6	rigid

the flexible colloidal lattice within this time. At $t=0$, a small number of small-sized clusters were already present within the sample (see Figure 4.1 and 4.4). This is due to a time delay of approximately 5 minutes between the mixing of particles and the acquisition of the first snapshot of the self-assembly process.

Upon mixing the colloidal particles, we observed the rapid growth of small clusters as seen in Figure 4.1. This initial growth phase was due to the high availability and fast diffusion of single particles which allows frequent interactions between single particles and small clusters. As the lattice structures continued to develop, the growth rate gradually slowed down, due to the reduced diffusivity of the growing clusters, and lattice growth became predominantly governed by the addition of single particles. However, we also identified instances of cluster-cluster growth, where aggregates of 2-3 particles contributed to the overall lattice development.

The surprising finding of floppy lattices with square bond topology stems from their ability to rearrange after binding. During the growth process, both spheres were able to access the full range of motion around the other particles species which allowed the particles to rearrange and optimise their location after binding. While the formed bonds are irreversible, the complementarily functionalized particles are able rearrange and continue to bind to other, already bound particles, thereby lowering their free energy. Surprisingly, these rearrangements lead to square-like arrangements consisting of rings of four particles with alternating DNA functionalization (see Figure 4.2a). Consecutively binding particles also frequently rearrange to form this basic unit, leading to structures that are preferentially square lattices. This is reminiscent of the three-dimensional CsCl structures obtained for colloids coated with surface bound DNA that were assembled close to their melting temperature.[12] However, the lattices obtained here are quasi-two dimensional. Since the connectivity is below isostaticity and because the bonds can rearrange, the lattice can possess floppy modes. For the square lattices, the floppy modes consist of shear modes that randomly switch back and forth between a square and hexagonal arrangement of particles (see Figure 4.2a and 4.3a). Thus,

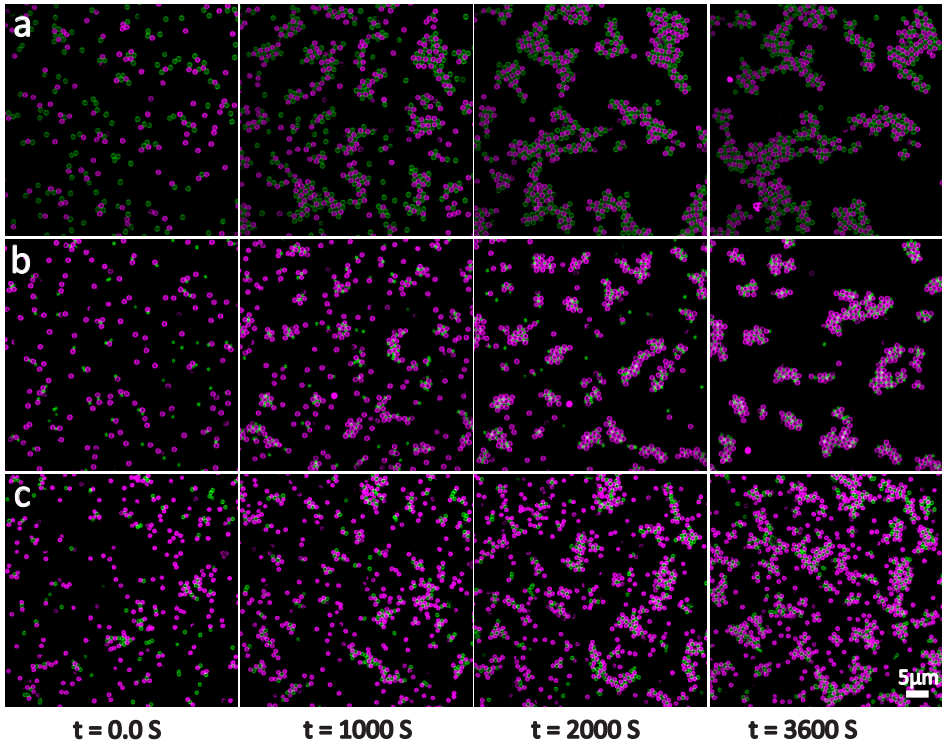


Figure 4.1: Self-assembly of flexible colloidal lattices. Representative confocal microscopy snapshots showing the self-assembly of a binary mixture of (a) equal sized spheres with diameter 2.06 ± 0.05 shown in magenta and 2.06 ± 0.05 shown in green (size ratio $\alpha_{s-s} = 1$) (b) unequal sized spheres with size ratio $\alpha_{s-s} = 1.65$ consisting of 2.06 ± 0.05 μm spheres shown in magenta and 1.25 ± 0.05 μm spheres shown in green, and (c) 1.66 ± 0.05 μm spheres shown in magenta and cubes with edge-length 1.35 ± 0.07 μm cubes shown in green of $\alpha_{s-c} = 1.23$. (a)-(c) Magenta and green color indicate functionalization with complementary DNA strands.

the rearranging bonds surprisingly help crystallization into an ordered structure, a square lattice, and are a prerequisite for the assembled structures to exhibit floppy modes.

Intrigued by the self-assembled floppy square lattices, we investigated if particle shape and size ratio can be leveraged to enhance the purity and yield of floppy square lattices further. To do so, we employed unequal sized spheres of 2.06 ± 0.05 μm with 1.25 ± 0.05 μm spheres of $\alpha_{s-s} = 1.65$ in a 1.2:1 number ratio, and 1.66 ± 0.05 μm spheres with 1.35 ± 0.07 μm cubes of $\alpha_{s-s} = 1.23$ in a 1:1 number ratio. These combinations of size ratio and particle shape were previously shown by some of us to lead to the preferential self-assembly of colloidal molecules with coordination number 4, the same coordination number that is needed for square lattices (see Figure 4.2b and c).[7, 17, 21]

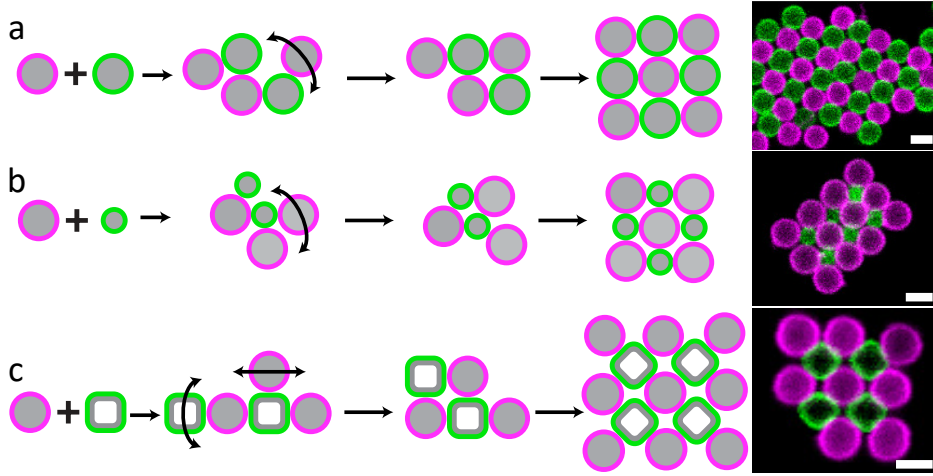


Figure 4.2: Schematic showing how reconfiguration during nucleation and growth leads to ordered, floppy structures, and their rearrangement based on their motion type during the assembly process. for a binary mixture of (a) equal sized spheres with $2.06 \pm 0.05 \mu\text{m}$ diameter, $\alpha_{s-s} = 1$; complementary DNA functionalization indicated in magenta and green. During the nucleation and growth both particles show the full range of motion with respect to other, allowing clusters to rearrange and optimise their position, which leads to the formation of square lattices. (b) unequal sized $2.06 \pm 0.05 \mu\text{m}$ (indicated in magenta) and $1.25 \pm 0.05 \mu\text{m}$ spheres (indicated in green) with $\alpha_{s-s} = 1.65$. Similar to $\alpha_{s-s} = 1$ both particles show the full range of motion with respect to other and form square lattices, enhanced by the size ratio that favors coordination of the smaller particles by four bigger particles. (c) spheres (diameter $1.66 \pm 0.05 \mu\text{m}$, indicated in magenta) and cubes (edge length $1.35 \pm 0.07 \mu\text{m}$, indicated in green) with $\alpha_{s-c} = 1.23$. During nucleation and growth, the spheres' motion is confined to the cubes' sides, while cubes show full range of motion on the spheres surface. The cubic symmetry enhances the formation of square lattices

We follow their assembly dynamics in time using confocal microscopy and again find the emergence of well-ordered structures with square topology, see Figure 4.1b. For spheres with size ratio $\alpha_{s-s} = 1.65$ the bond flexibility and spherical shape again allows the spheres to have a full range of motion relative to each other. This characteristic enables the particles to reconfigure similar to $\alpha = 1$, however, the geometric constraint imposed by the different size ratio $\alpha_{s-s} = 1.65$ permits binding of a maximum of four $2.06 \mu\text{m}$ particles per $1.25 \mu\text{m}$ sphere thereby increasing the probability to form square lattices. Despite the spatial constraints imposed by the size difference, the lattice maintains its flexibility and overall configuration, see Figure 4.3b.

Introducing a cubic shape we can further guide the assembly pathway towards square lattices. We have previously shown that using a combination of cubes and spheres constrains the motion of the spheres to the cubes' sides above a critical size ratio strongly favoring a coordination with four spheres in quasi 2D systems.

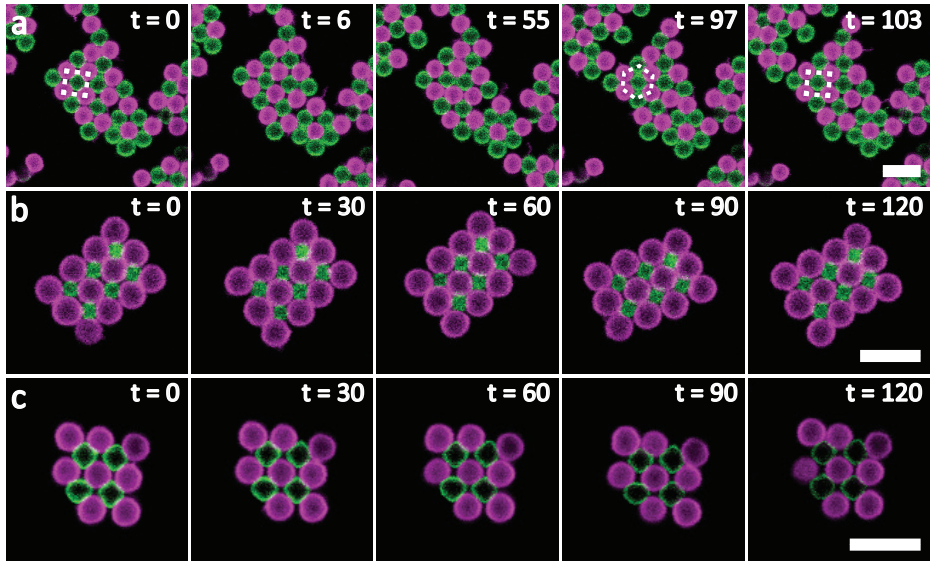


Figure 4.3: Confocal microscopy snapshots of a time series showing the temperature-induced shape changes of the self-assembled lattice. (a) Shows the local transition of square (indicated by square dotted box) to hexagonal lattice (indicated by dotted hexagonal box) with time for equal sized spheres of $2.06 \pm 0.05 \mu\text{m}$ and $2.06 \pm 0.05 \mu\text{m}$ ($\alpha_{s-s} = 1$). (b) Shows the unequal sized spheres of $2.06 \pm 0.05 \mu\text{m}$ and $2.06 \pm 0.05 \mu\text{m}$ ($\alpha_{s-s} = 1.65$) retain their square configuration over time. (c) Shows the spheres and cubes lattice of $1.66 \pm 0.05 \mu\text{m}$ and $1.35 \pm 0.05 \mu\text{m}$ ($\alpha_{s-c} = 1.23$) small shape changes while maintaining there square configuration over time. Scale bar is $5 \mu\text{m}$. Time t is in seconds.

[17] This confinement restricts the degrees of freedom for the spheres and thereby enhances the accuracy and yield of the square lattices, see Figure 4.1c. At the same time, the sliding motion of the spheres on the cubes leads to lattices with a different and more limited flexibility as shown in figure 4.3c.

To get quantitative information about the growth of the clusters, we extracted cluster size evolution over time from tracking the x and y position of the particles, see methods. Due to the limitations in the speed of capturing frames, particles diffuse over a distance larger than their radius between the frames, making it impossible to identify particle trajectories.

The number of particles within a cluster is then calculated using a cut-off distance-based clustering method. This method counts particles as belonging to a cluster if their separation is less than or equal to a predetermined cut-off distance, which is approximately equal to the sum of the radii of both particles. When plotting cluster size as a function of time, we observe fluctuations in all examined cases, see Figure 4.4. This can be attributed to the used cut-off method, which counts particles as belonging to a cluster if they are closer than a predetermined distance threshold, even if they are not bonded to it and leave the cluster at a later time. For the assembly of spheres and cubes, the center to center distance

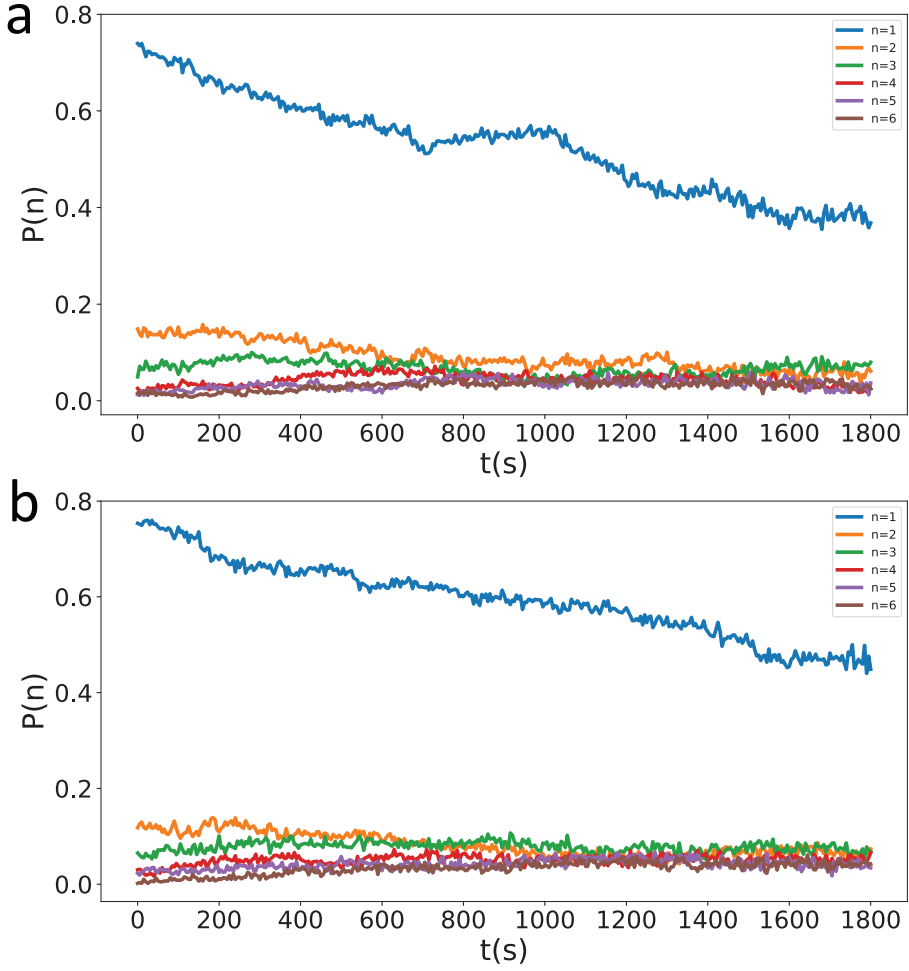


Figure 4.4: Probability of finding flexible colloidal clusters of size n over time. (a) Cluster growth of equal sized spheres with $\alpha_{s-s} = 1$ up to $n=6$. (b) Cluster growth of unequal sized spheres of $\alpha_{s-s} = 1.65$ up to $n=6$.

between cube and sphere changes with the position of the sphere on the cube, making it difficult to define a unique cut-off distance. Since extracting the cubes' orientation is challenging, we could not plot the cluster size evolution with time for this case.

Figure 4.1 and 4.4 reveal that the rate of lattice growth is significantly influenced by the size and shape of the building blocks. Specifically, we observed that the crystallization kinetics are faster for equal sized spheres of $\alpha_{s-s} = 1$ compared to unequal sized spheres of $\alpha_{s-s} = 1.65$, and spheres and cubes of $\alpha_{s-c} = 1.23$. While the faster diffusion for the smaller particles for $\alpha_{s-s} = 1.65$ and $\alpha_{s-c} = 1.23$ should lead to quicker self-assembly since the time required for particles to meet and interact is shorter, we find that their assembly is slower compared to that of equal sized spheres. This can be rationalized considering that our choice of weak multivalent bonds requires a particle to stay in close proximity to its complementary particle for an extended period of time before binding occurs between multiple linkers. The higher diffusivity thus results in a lower probability of binding and slower self-assembly. Additionally, the higher gravitational height of the smaller spheres and cubes allows particles to diffuse in 3D lowering the probability for interaction and resulting in slower assembly compared to the larger spheres used for $\alpha_{s-s} = 1$. This highlights the importance of particle size in determining the lattice growth kinetics.

4.3.2 Crystallisation Pathways of Flexible Colloidal Lattices

To understand more about the growth kinetics and reconfiguration of flexible colloidal lattices, we now analyse the assembly pathways of our binary mixture of colloids taking possible reconfigurations into account. From the tracked x, y position of the individual particles and the cluster size n , we generated the adjacency matrices for each cluster size and type. These matrices allowed us to identify and distinguish clusters of the same size but with different bond topology by their eigenvalues.

Our analysis of the growth kinetics of flexible colloidal lattices reveals a series of pathways in cluster configurations and variety of distinct cluster types as they increase in size n . Therefore, we restrict our analysis up to a $n=6$. For equal size spheres of $\alpha_{s-s} = 1$, initially, particles form $n=2$ and $n=3$ clusters. By addition of a single particle indicated by the white arrow in Figure 4.5, they evolve into $n=4$ with three distinct types of shapes. This is the first cluster size where reconfiguration can change the topology from a chain to a square. If the growth continues by addition of a single particle, these clusters transform into $n=5$ with 4 distinct types of shapes as seen in Figure 4.5. When n reaches six, there are twelve distinct types of cluster shapes. From $n=4$ onward, reconfiguration of cluster occurs to that do not maximise the number of possible bonds yet into stable cluster as indicated by the red arrow in Figure 4.5. Extracting all cluster types of a particular n from microscope images is not possible due to the small field of view captured from large sample. Therefore, we show representative cluster types in Figure 4.5.

For unequal sized spheres of $\alpha_{s-s} = 1.65$ as shown in Figure 4.6 cluster shapes identical to $\alpha_{s-s} = 1$ are seen up to $n=4$. The different size ratio on the one hand

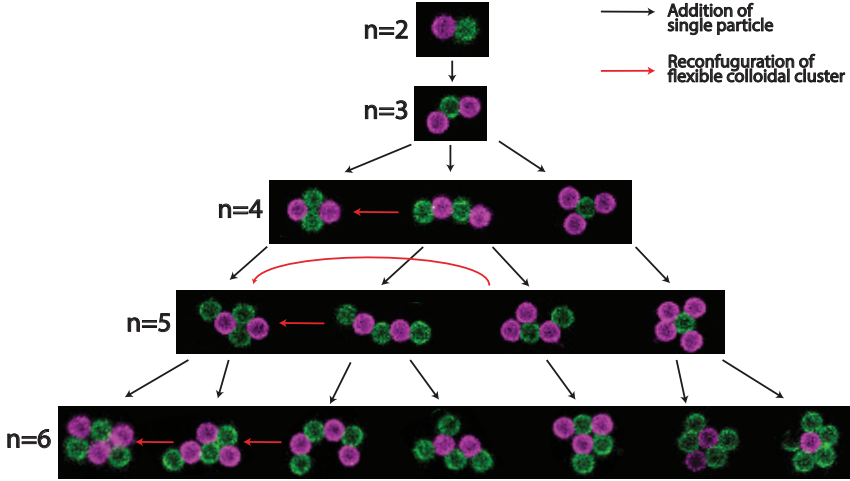


Figure 4.5: Assembly pathways of flexible colloidal structures for $\alpha_{s-s} = 1$. Confocal microscopy snapshots of flexible colloidal clusters of size $n=2-6$ consisting of $2.06 \pm 0.05 \mu\text{m}$ spheres (displayed in magenta) and $2.06 \pm 0.05 \mu\text{m}$ spheres (displayed in green) and their pathways taken to assemble into various clusters of size n by the addition of single particles (black arrows) and through reconfiguration (red arrows).

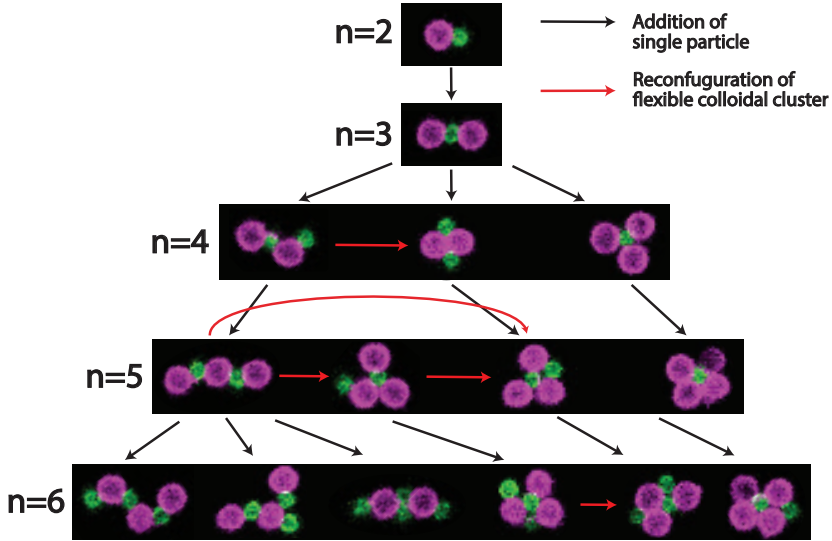


Figure 4.6: Assembly pathways of flexible colloidal structures $\alpha_{s-s} = 1.65$. Confocal microscopy snapshots of pathways of flexible colloidal clusters of size $n=2-6$ consisting of $2.06 \pm 0.05 \mu\text{m}$ spheres (displayed in magenta) and $1.25 \pm 0.05 \mu\text{m}$ spheres (displayed in green) and their pathways taken to transform into various clusters size n and types by the addition of single particles (black arrows) and through reconfiguration (red arrows).

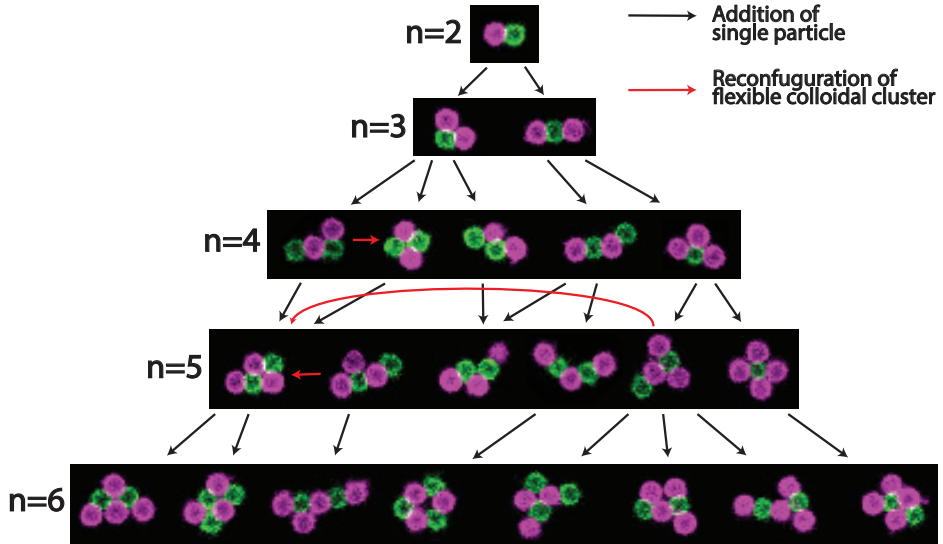


Figure 4.7: Assembly pathways of flexible colloidal structures $\alpha_{s-c} = 1.23$. Confocal microscopy snapshots depicting the pathways of flexible colloidal clusters of size $n=2-6$ consisting of $1.66 \pm 0.05 \mu\text{m}$ spheres (displayed in magenta) and $1.35 \pm 0.07 \mu\text{m}$ cubes (displayed in green) of $\alpha_{s-s} = 1.23$ and their pathways taken to transform into various clusters size n and types by the addition of single particles (black arrows) and through reconfiguration (red arrows).

increases the number of shapes as the particles are now distinguishable. On the other hand, it imposes different geometric constraints, that is, at maximum four large spheres can bind on a smaller one whereas eight small spheres can bind on each larger one. Again, reconfigurations between additions of particles increase the number of bonds and often lead to closed loops of four particles. Finally, using cubes instead of spheres significantly affects the assembly pathways. The reason is that the cubic shape at this size ratio restricts the motion of the spheres to the side they first absorb onto. This implies more distinctly different states for a given cluster size n while at the same time restricting reconfiguration to motion of cubes on spheres but not vice versa (see Figure 4.7). The directional bonds induced by the cubic shape inherently lead to a lattice with square symmetry.

4.3.3 Characterisation of Flexible Colloidal Lattices

Analyzing the arrangement of colloidal particles within the two-dimensional flexible colloidal lattices provides a better understanding of the effect of size and shape on degree of flexibility and the final structure of flexible colloidal lattices. To do so, we measure the number of bonds per particle in the lattice usually called coordination number and denoted by Z_c , the bond angle distribution, and the local bond order parameter ($\psi_{i,6}$) of lattices.

As depicted in Figure 4.8a, we extracted the x and y coordinates of all particles,

calculated the coordination number (Z_c), and plotted their position with color-coded values of Z_c . For equal sized spheres, the analyzed structure is shown in Figure 4.8a, and the corresponding plot of the coordination number in Figure 4.8b. The distribution of the coordination number (Z_c) shown in Figure 4.8c reveals that for $\alpha = 1$, Z_c ranges from 1 to 5 with a peak at 3. This is in line with our expectation for small crystalline grains since particles at an edge mostly have $Z_c=3$, while inner particles have $Z_c=4$, and corners have $Z_c=2$.

For the binary spheres with $\alpha_{s-s} = 1.65$ designed to form square symmetry we calculate Z_c only for the smaller particles (green). Then, Z_c is between 1 to 4, with a peak at 4 as shown in 4.9a, b, and c, clearly indicating the geometric constraints imposed by our deliberate choice of the size ratio. For the cube-sphere system, Z_c ranged from 1 to 4, with a peak at 3, as can be seen in Figure 4.10a, b, and c. The edges of these small crystalline grains have $Z_c=3$, inner particles have $Z_c=4$, and corners have $Z_c=2$. Overall, the visual observation of square lattices should imply an average of $Z_c \leq 4$ on the inside of the crystalline grains. This indeed can be seen in Figures 4.8b, 4.9b and 4.10b. The presence of edges and corners lowers the average coordination number, leading to a peak at 3. Thus, the results from our quantitative analysis of Z_c are in line with the square lattice geometry. However, Z_c provides limited information about the local order of the crystalline grains due to their small sizes. In order to gain a better understanding of the local order of lattices, we calculate the angle between adjacent particles and the local bond order parameter, which provides a quantitative and comprehensive analysis of the lattice structure.

Figure 4.11a, 4.12a and 4.13a show bond angle distributions for equal size spheres with $\alpha_{s-s} = 1$, unequal size spheres with $\alpha_{s-s} = 1.65$ and spheres and cubes with $\alpha_{s-c} = 1.23$, respectively. Since the square symmetry of the lattices is visible in Figures 4.8, 4.9 and 4.10, we expect for all three cases that the average bond angle distribution peaks at $\approx 90^\circ$ which agrees with our measurements shown in Figure 4.11a, 4.12a and 4.13a. Bond angles around 180° stem from edge and corners particles with $Z_c=2$ and 3. This further supports the presence of four-fold symmetry in the system. We also find that the bond angle distribution gets more narrow by imposing geometric constraints in case of $\alpha_{s-s} = 1.65$. For the combination of cubes and spheres the confinement of the spheres to the cubes sides enhances the effect.

Another approach to quantitatively determine the degree of orientational order among neighboring particles is by calculating the local bond order parameter. A value of 1 indicates that the lattice structures are perfectly ordered, while a value of 0 indicates a disordered or liquid-like structure. A local order parameter analogous to $\psi_{i,6}$ can be calculated for four-fold symmetry $\psi_{i,4}$ using the following equation:

$$\psi_{i,4} = \frac{1}{N_i} \sum_{j=1}^{N_i} \exp(4i\theta_j)$$

Here, N_i is the number of bonds in the i th ring around the center particle, and θ_j is the angle between a fixed reference neighbor and the vector pointing from the j th particle (center particle) to its nearest neighbor in the ring. $\psi_{i,4}$ value is set to 0 for particles with only one nearest neighbor. The angle between the nearest

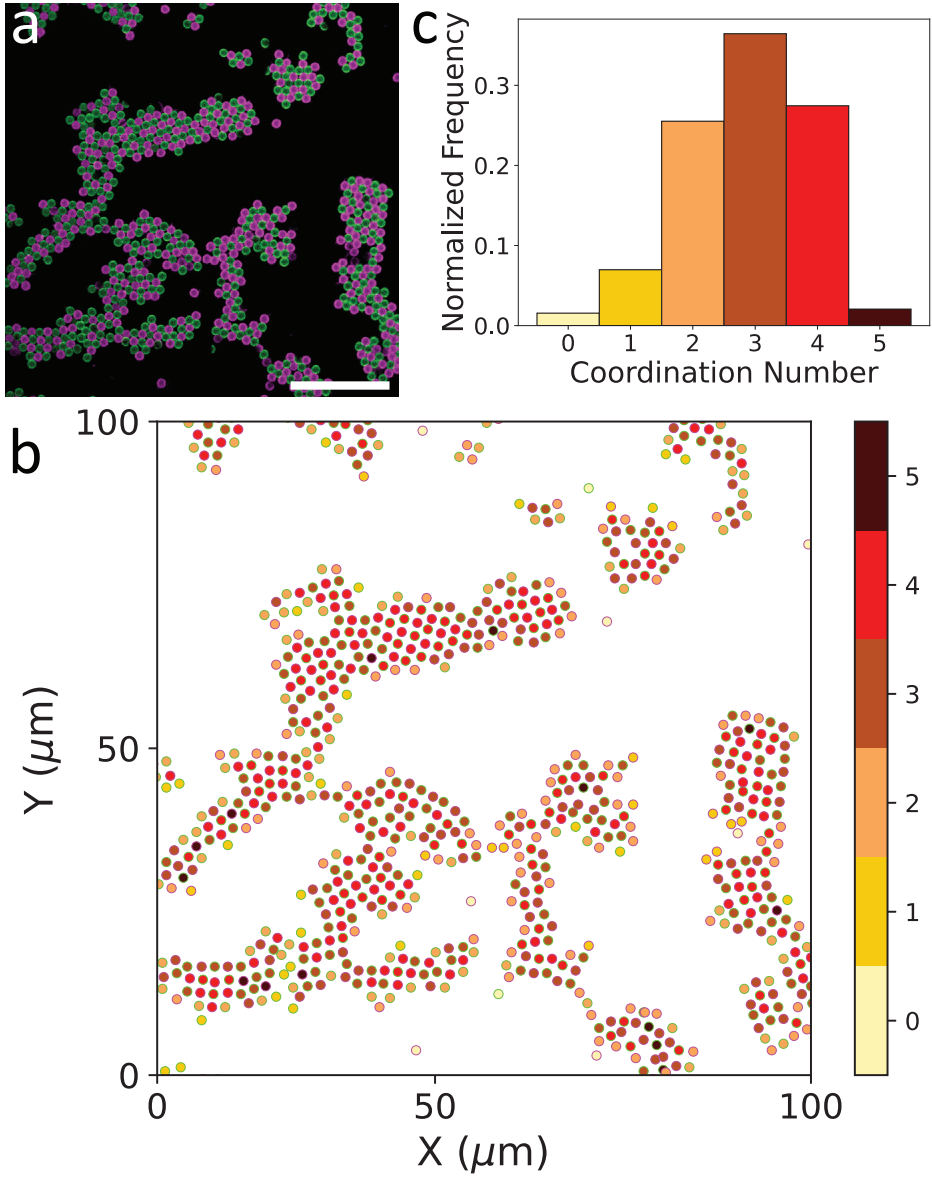


Figure 4.8: Analysis of the number of bonds in flexible colloidal lattices composed of equal sized spheres of $2.06 \mu\text{m}$ diameter. (a) Confocal image of the flexible colloidal lattices. Scale bar is $25 \mu\text{m}$ (b) Color-coded graphic represents the number of bonds with green and magenta rings filled with color denote the number of bonds for green and magenta particles, respectively. (c) A plot illustrating the relationship between the number of bonds and normalized frequency.

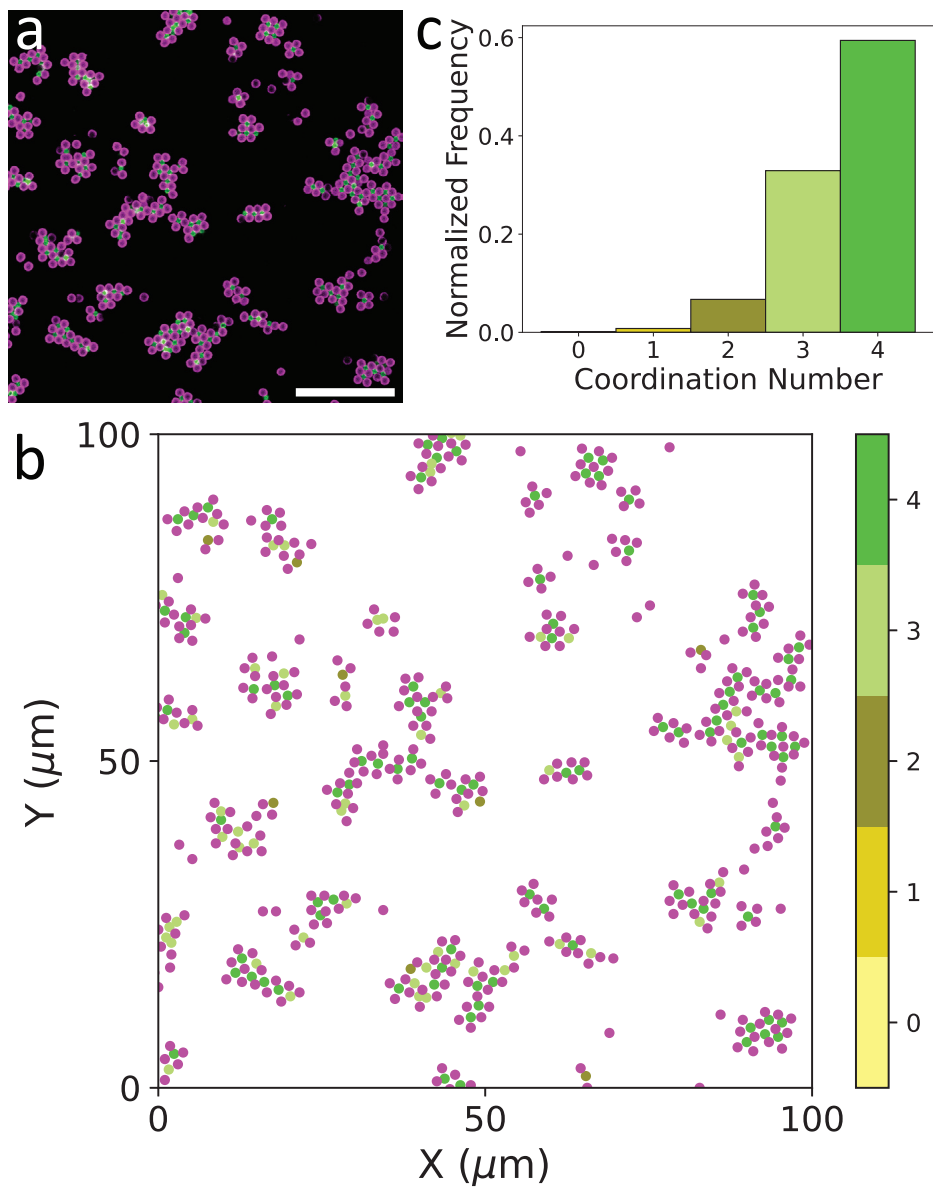


Figure 4.9: Analysis of the number of bonds in flexible colloidal lattices composed of un-equal sized spheres of size $2.06 \mu\text{m}$ and $1.25 \mu\text{m}$. (a) Confocal image of the flexible colloidal lattices. Scale bar is $25 \mu\text{m}$. (b) Color-coded graphic represents the number of bonds with green rings filled with color denote the number of bonds for green particles, respectively. (c) A plot illustrating the relationship between the number of bonds and normalized frequency.

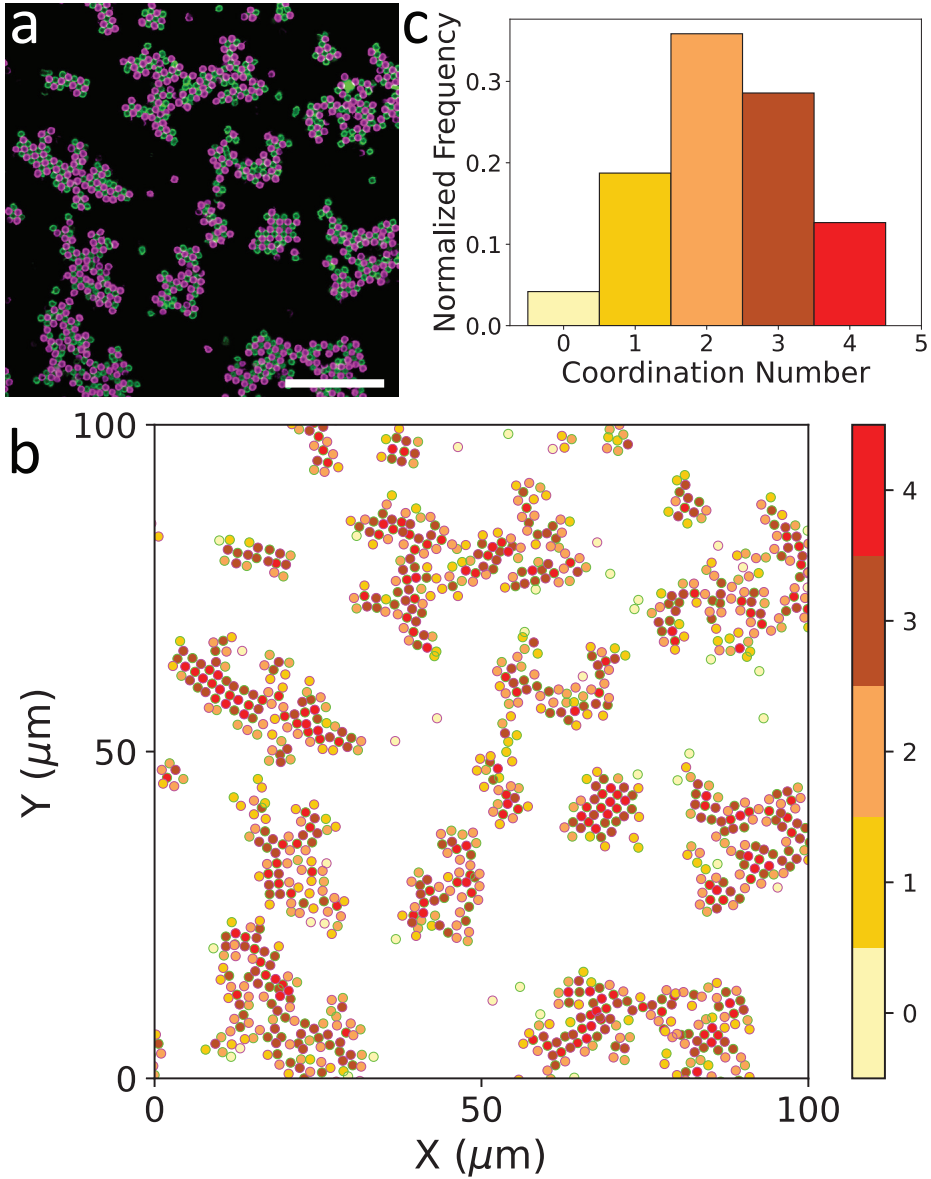


Figure 4.10: Analysis of the number of bonds in flexible colloidal lattices composed of $1.66 \mu\text{m}$ spheres and $1.35 \mu\text{m}$ cubes. (a) Confocal image of the flexible colloidal lattices. Scale bar is $25 \mu\text{m}$. (b) Color-coded graphic represents the number of bonds with green and magenta rings filled with color denote the number of bonds for green and magenta particles, respectively. (c) A plot illustrating the relationship between the number of bonds and normalized frequency.

neighbours can then be calculated using the following equation:

$$\theta_j = \text{atan2}(\|\mathbf{u} \times \mathbf{v}\|, \mathbf{u} \cdot \mathbf{v})$$

where \mathbf{u} is the vector pointing from the central particle to its nearest neighbors and \mathbf{v} is the vector pointing from the central particle to a fixed reference neighbour.

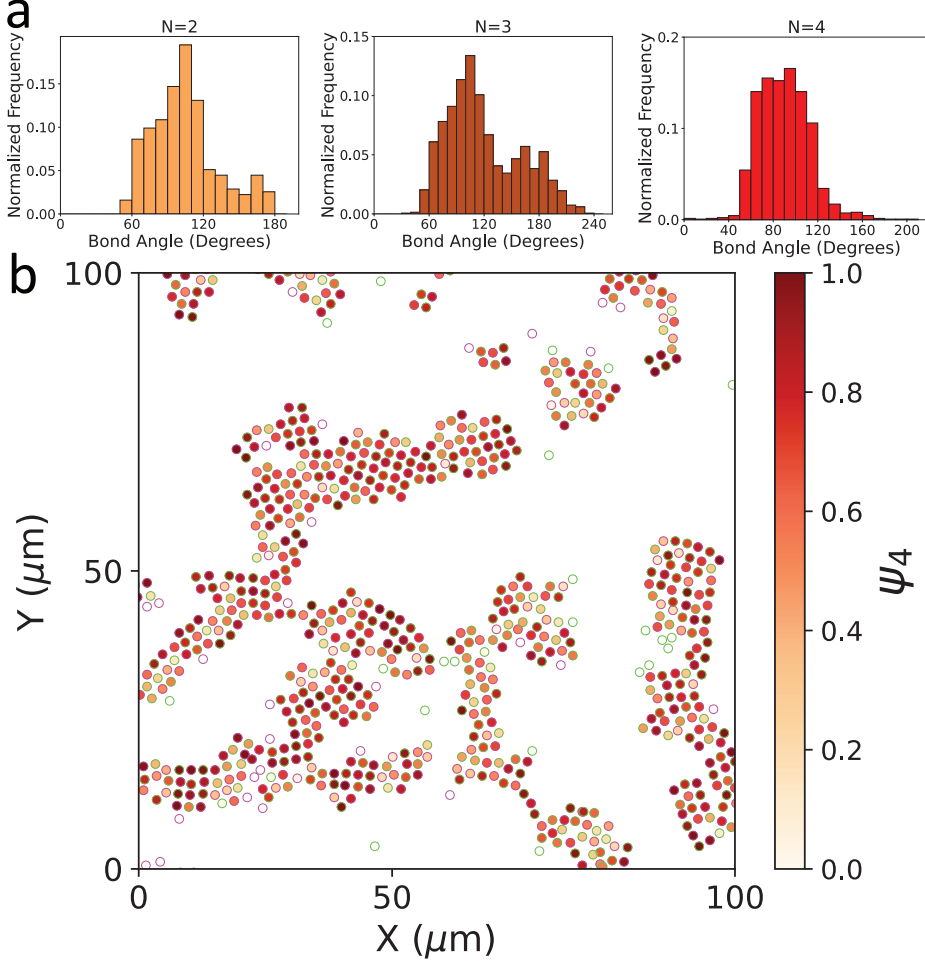


Figure 4.11: (a) Bond angle distribution for spheres with N neighbors and (b) Local bond order parameter analysis of flexible colloidal lattices consisting of $2.06 \mu\text{m}$ spheres ($\alpha_{s-s} = 1$).

We analyze the local bond parameter for equal sized spheres of $\alpha_{s-s} = 1$ in Figure 4.11b, unequal sized spheres of $\alpha_{s-s} = 1.65$ in Figure 4.12b, and spheres-cubes of $\alpha_{s-c} = 1.23$ in Figure 4.13b. For $\alpha_{s-s} = 1$, the plot in Figure 4.11b shows that the system has a wide distribution of bond angles, indicating a less ordered crystalline structure. This can be attributed to the equal size of spheres

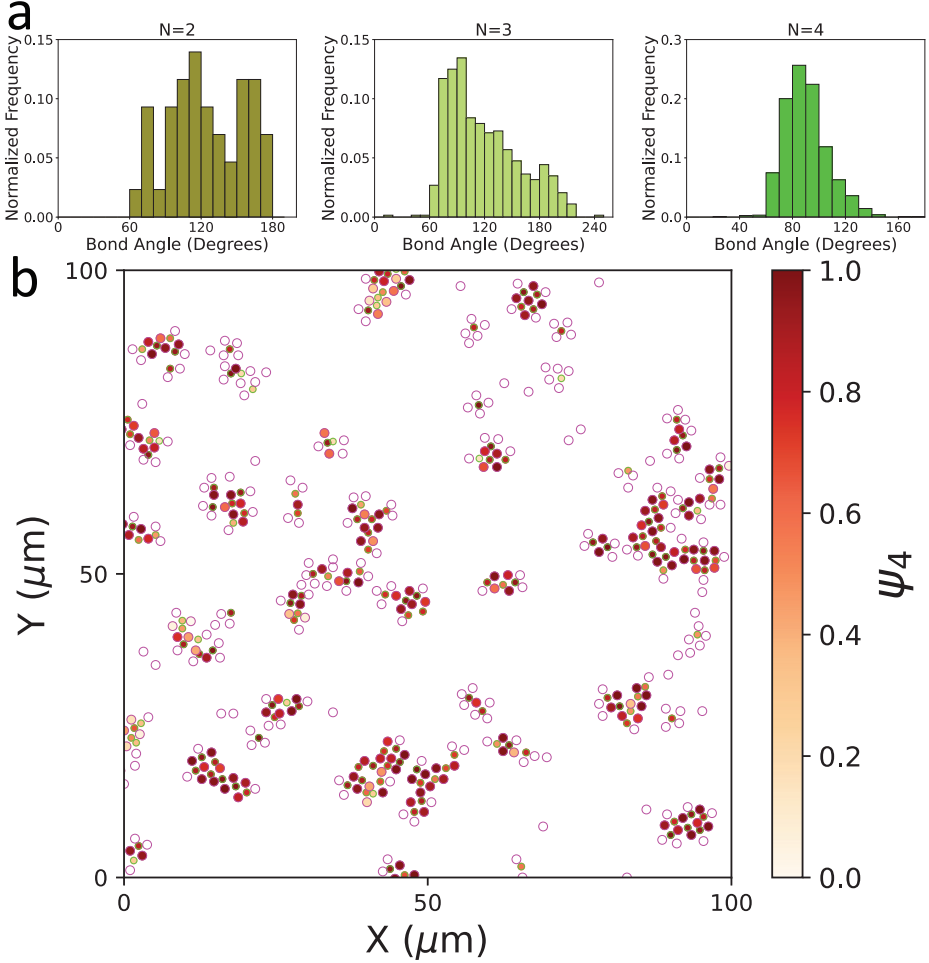


Figure 4.12: (a) Bond angle distribution for spheres with N neighbors and (b) Local bond order parameter analysis of flexible colloidal lattices consisting of 2.06 μm and 1.25 μm spheres ($\alpha_{s-s} = 1.65$).

and their isotropic shape, which allows for greater variation in bond angles and more freedom for the spheres to move. On the other hand, for unequal size spheres of $\alpha_{s-s} = 1.65$, one might expect an increase in the order of the system due to the presence of different sphere sizes which impose geometric constraints. However, the graph in Figure 4.12b shows a decrease in order as $\psi_{i,4}$ is calculated considering both big and small spheres. However assembly proceeded slower and thus the size of the analyzed lattices are smaller compared to $\alpha_{s-s} = 1$ and $\alpha_{s-s} = 1.65$. Therefore, it may only provide limited information about its orientational order. Lastly, the lattice assembled from spheres and cubes exhibit a higher degree of order compared to both binary sphere systems with $\alpha_{s-s} = 1$ and $\alpha_{s-s} = 1.65$. This increased order can be attributed to the geometric constraints and confined

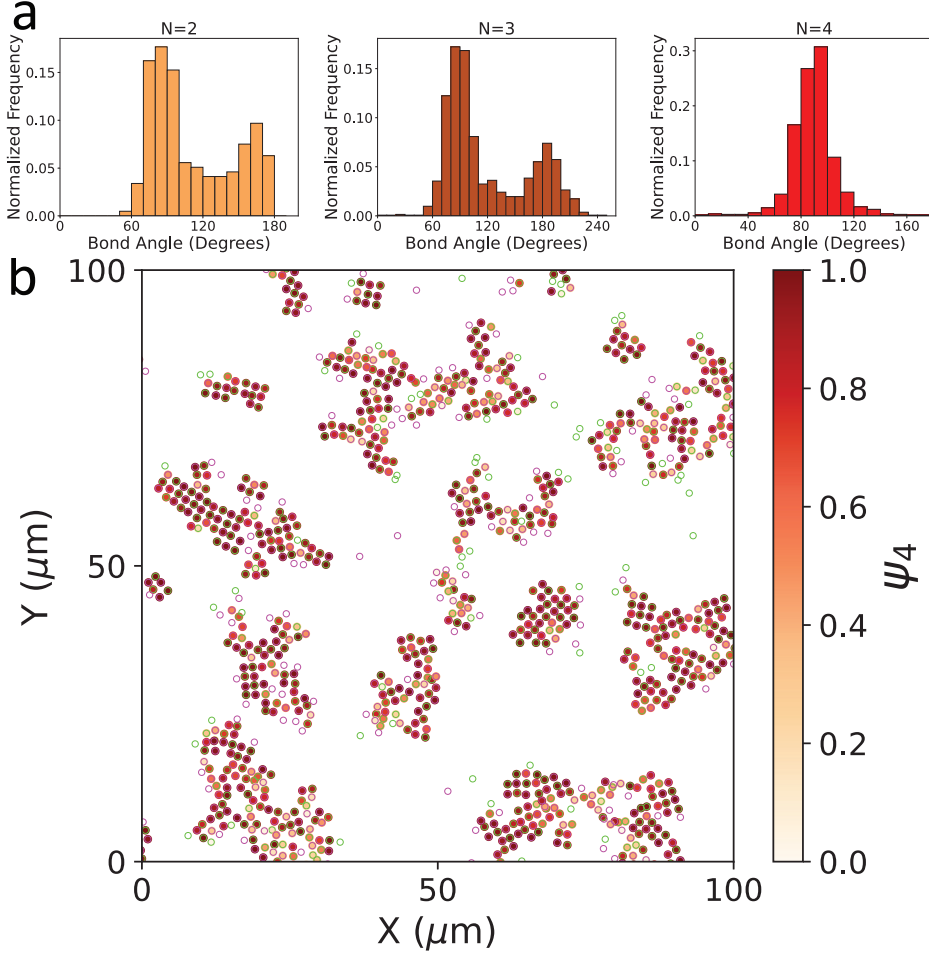


Figure 4.13: (a) Bond angle distribution for spheres with N neighbors and (b) Local bond order parameter analysis of flexible colloidal lattices consisting of $1.66 \mu\text{m}$ spheres and $1.35 \mu\text{m}$ cubes ($\alpha_{s-c} = 1.23$).

motion of the spheres on the cube faces.

4.4 Conclusions

In this study, we demonstrated the self-assembly of binary mixtures of colloidal particles functionalized with surface-mobile DNA into flexible square colloidal lattices. Our findings indicate that when equal-sized spheres are used, the self-assembled lattice exhibits a dynamic local transition between square and hexagonal configurations. In contrast, when using unequal-sized spheres, the lattice maintains a square arrangement due to geometric constraints imposed by the different size ratio, while maintaining flexibility. Additionally, we observed that the lattice composed of a combination of spheres and cubes retains a square lattice structure with limited angular motion resulting from the confined movement of spheres over the cubes' surfaces.

Through image analysis of the growth kinetics of flexible colloidal lattices, we discovered that the system with equal-sized spheres exhibits the fastest growth over time, while the system comprising spheres and cubes takes the longest time to self-assemble into square flexible lattices. We also found that the system with unequal-sized spheres has the fewest number of pathways to assemble into flexible lattices, whereas the introduction of geometric constraints and confined flexibility results in the highest number of pathways.

Our results suggest that a system composed of large and small spheres provides the optimal configuration for obtaining square lattices albeit with limited flexibility without sacrificing lattice symmetry. By calculating the local bond order parameter, we determined that the combination of geometric constraints and confined flexibility in the system of spheres and cubes yields the most locally ordered lattice structures. Our findings demonstrate that particle shape, size, and reconfiguration play crucial roles in nucleation and growth, time required for formation of the lattices and determining the lattice arrangement. These results may serve as a valuable tool for selecting the appropriate building shape, size and motion type to design flexible colloidal materials with customized properties.

Acknowledgements

I am grateful to Daniel J.G. Pearce (University of Geneva) for fruitful discussions. I thank Rachel Doherty for SEM imaging and Christine Linne for assistance with DNA design. I also thank Ali Azadbhakt, Julio Melio, Solenn Riedel and Samdarshi Maity for their help with Python coding and valuable discussions.

4.5 Bibliography

- [1] Jennifer J Williams, Christopher W Smith, Kenneth E Evans, Zoe AD Lethbridge, and Richard I Walton. Off-axis elastic properties and the effect of extraframework species on structural flexibility of the nat-type zeolites: simulations of structure and elastic properties. *Chemistry of Materials*, 19(10):2423–2434, 2007.
- [2] Wenbo Wu, Kui Chen, Ting Wang, Na Wang, Xin Huang, Lina Zhou, Zhao Wang, and Hongxun Hao. Stimuli-responsive flexible organic crystals. *Journal of Materials Chemistry C*, 2023.
- [3] Yuan Wang, Lei Yang, Xiao-Lei Shi, Xun Shi, Lidong Chen, Matthew S Dargusch, Jin Zou, and Zhi-Gang Chen. Flexible thermoelectric materials and generators: challenges and innovations. *Advanced Materials*, 31(29):1807916, 2019.
- [4] Xiluan Wang and Gaoquan Shi. Flexible graphene devices related to energy conversion and storage. *Energy & Environmental Science*, 8(3):790–823, 2015.
- [5] Gamidi Rama Krishna, Ramesh Devarapalli, Garima Lal, and C Malla Reddy. Mechanically flexible organic crystals achieved by introducing weak interactions in structure: supramolecular shape synthons. *Journal of the American Chemical Society*, 138(41):13561–13567, 2016.
- [6] Frank Smallenburg and Francesco Sciortino. Liquids more stable than crystals in particles with limited valence and flexible bonds. *Nature Physics*, 9(9):554–558, 2013.
- [7] Indrani Chakraborty, Daniel JG Pearce, Ruben W Verweij, Sabine C Matysik, Luca Gioni, and Daniela J Kraft. Self-assembly dynamics of reconfigurable colloidal molecules. *ACS Nano*, 16(2):2471–2480, 2022.
- [8] Carolyn L Phillips, Eric Jankowski, Bhaskar Jyoti Krishnatreya, Kazem V Edmond, Stefano Sacanna, David G Grier, David J Pine, and Sharon C Glotzer. Digital colloids: reconfigurable clusters as high information density elements. *Soft Matter*, 10(38):7468–7479, 2014.
- [9] Stef AJ van der Meulen and Mirjam E Leunissen. Solid colloids with surface-mobile dna linkers. *Journal of the American Chemical Society*, 135(40):15129–15134, 2013.
- [10] Indrani Chakraborty, Vera Meester, Casper van der Wel, and Daniela J Kraft. Colloidal joints with designed motion range and tunable joint flexibility. *Nanoscale*, 9(23):7814–7821, 2017.
- [11] Angus McMullen, Miranda Holmes-Cerfon, Francesco Sciortino, Alexander Y Grosberg, and Jasna Brujic. Freely jointed polymers made of droplets. *Physical Review Letters*, 121(13):138002, 2018.

- [12] Yu Wang, Yufeng Wang, Xiaolong Zheng, Étienne Ducrot, Jeremy S Yodh, Marcus Weck, and David J Pine. Crystallization of dna-coated colloids. *Nature Communications*, 6(1):7253, 2015.
- [13] Jeongbin Moon, In-Seong Jo, Etienne Ducrot, Joon Suk Oh, David J Pine, and Gi-Ra Yi. Dna-coated microspheres and their colloidal superstructures. *Macromolecular Research*, 26(12):1085–1094, 2018.
- [14] Ruben W Verweij, Pepijn G Moerman, Nathalie EG Ligthart, Loes PP Huijnen, Jan Groenewold, Willem K Kegel, Alfons van Blaaderen, and Daniela J Kraft. Flexibility-induced effects in the brownian motion of colloidal trimers. *Physical Review Research*, 2(3):033136, 2020.
- [15] Ruben W Verweij, Pepijn G Moerman, Loes PP Huijnen, Nathalie EG Ligthart, Indrani Chakraborty, Jan Groenewold, Willem K Kegel, Alfons van Blaaderen, and Daniela J Kraft. Conformations and diffusion of flexibly linked colloidal chains. *Journal of Physics: Materials*, 4(3):035002, 2021.
- [16] Ruben W Verweij, Julio Melio, Indrani Chakraborty, and Daniela J Kraft. Brownian motion of flexibly linked colloidal rings. *Physical Review E*, 107(3):034602, 2023.
- [17] Yogesh Shelke, Fabrizio Camerin, Susana Marín-Aguilar, Ruben W. Verweij, Marjolein Dijkstra, and Daniela J. Kraft. Flexible colloidal molecules with directional bonds and controlled flexibility. *ACS Nano*, 17(13):12234–12246, 2023.
- [18] Tadao Sugimoto and Kazuo Sakata. Preparation of monodisperse pseudocubic α - Fe_2O_3 particles from condensed ferric hydroxide gel. *Journal of Colloid and Interface Science*, 152(2):587–590, 1992.
- [19] Yong Wang, Xiaowen Su, Panshuang Ding, Shan Lu, and Huaping Yu. Shape-controlled synthesis of hollow silica colloids. *Langmuir*, 29(37):11575–11581, 2013.
- [20] Melissa Rinaldin, Ruben W Verweij, Indrani Chakraborty, and Daniela J Kraft. Colloid supported lipid bilayers for self-assembly. *Soft Matter*, 15(6):1345–1360, 2019.
- [21] Yogesh Shelke, Susana Marín-Aguilar, Fabrizio Camerin, Marjolein Dijkstra, and Daniela J Kraft. Exploiting anisotropic particle shape to electrostatically assemble colloidal molecules with high yield and purity. *Journal of Colloid and Interface Science*, 629:322–333, 2023.

